

Direct detection of natural selection in Bronze Age Britain

Iain Mathieson¹ and Jonathan Terhorst²

¹Department of Genetics, Perelman School of Medicine, University of Pennsylvania, Philadelphia, Pennsylvania 19104, USA;

²Department of Statistics, University of Michigan, Ann Arbor, Michigan 48109, USA

We developed a novel method for efficiently estimating time-varying selection coefficients from genome-wide ancient DNA data. In simulations, our method accurately recovers selective trajectories and is robust to misspecification of population size. We applied it to a large data set of ancient and present-day human genomes from Britain and identified seven loci with genome-wide significant evidence of selection in the past 4500 yr. Almost all of them can be related to increased vitamin D or calcium levels, suggesting strong selective pressure on these or related phenotypes. However, the strength of selection on individual loci varied substantially over time, suggesting that cultural or environmental factors moderated the genetic response. Of 28 complex anthropometric and metabolic traits, skin pigmentation was the only one with significant evidence of polygenic selection, further underscoring the importance of phenotypes related to vitamin D. Our approach illustrates the power of ancient DNA to characterize selection in human populations and illuminates the recent evolutionary history of Britain.

[Supplemental material is available for this article.]

Ancient DNA (aDNA) provides direct insight into human evolutionary history. So far, this information has mainly been used to study demographic history—the migrations, splits, and admixtures that humans experienced in the recent past (Skoglund and Mathieson 2018). But, in principle, aDNA can also tell us about phenotypic evolution and, in particular, about the contribution of natural selection to phenotypic and genomic variation. Compared with demographic inference, this is more challenging, because studies of natural selection typically require larger sample sizes than studies of population history, which can integrate information from across the genome.

Although some recent studies have used aDNA to study selection and phenotypic evolution, they have mostly focused on a relatively small number of loci (e.g., Wilde et al. 2014; Mathieson and Mathieson 2018; Kerner et al. 2021). Studies that performed genome-wide scans for selection using aDNA (Mathieson et al. 2015; Skoglund et al. 2017; Margaryan et al. 2020) have compared allele frequencies across populations but have not made use of the precise temporal information available from direct dating of ancient samples. For example, the approach of Mathieson et al. (2015) was able to detect selection that happened some time in the past 8000 yr, somewhere in Western Eurasia, but could not be more specific.

With the recent publication of large aDNA data sets (e.g., Olalde et al. 2019; Margaryan et al. 2020; Patterson et al. 2022), sample sizes for some regions are now in the hundreds of individuals, large enough to study selection with good spatial and temporal resolution. However, there is a lack of suitable methods to analyze these data. There are many published methods for estimating selection coefficients from time series data (e.g., Bollback et al. 2008; Malaspina et al. 2012; Mathieson and McVean 2013; Feder et al. 2014; Lacerda and Seoighe 2014; Steinrücken et al. 2014;

Terhorst et al. 2015; Tataru et al. 2017), but all of them unrealistically assume that selective pressures are constant over time, and most are too slow to run on millions of markers at once. We therefore developed a novel statistical approach that is able to estimate arbitrary time-varying selection coefficients while being fast enough to run genome-wide.

The population of Britain, from 4500 yr before present (BP; i.e., the start of the Bronze Age) to the present day is ideal to show this approach for several reasons. First, it is relatively homogeneous in terms of both genetics and environment. Second, it is the population with the largest aDNA sample size. Third, there is a large amount of data about the genetic basis of complex traits in this population owing to analysis of the UK Biobank. Finally, one of the few studies that attempted to detect selection over this time period (based on data from present-day individuals) was performed in this population (Field et al. 2016), giving us a point of comparison for our aDNA-based approach.

Methods

We begin by formally defining the data, the inference problem, and the model we used to solve it. Our model is a generalization of the one used by Mathieson and McVean (2013). We assume a haploid Wright–Fisher (WF) population model whose size t generations before present was $2N_t$. Time runs backward, so that $t=0$ is the present, and $t=T$ is the earliest point where we have data. We are interested in the frequency of a single allele with two types A and a . In generation t , the a allele has relative fitness $1+s_t/2$ relative to A . Our inferential target is the vector $\mathbf{s} = (s_0, \dots, s_T)$ of selection coefficients over time. The population size history (N_0, \dots, N_T) is also allowed to vary with time, but we assume that it is known and do not attempt to jointly estimate it with \mathbf{s} .

© 2022 Mathieson and Terhorst. This article is distributed exclusively by Cold Spring Harbor Laboratory Press for the first six months after the full-issue publication date (see <https://genome.cshlp.org/site/misc/terms.xhtml>). After six months, it is available under a Creative Commons License (Attribution-NonCommercial 4.0 International), as described at <http://creativecommons.org/licenses/by-nc/4.0/>.

Corresponding authors: mathi@pennmedicine.upenn.edu,
jonth@umich.edu

Article published online before print. Article, supplemental material, and publication date are at <https://www.genome.org/cgi/doi/10.1101/gr.276862.122>.

The data consist of pairs of counts $\{(a_t, n_t)\}_{t=0}^T$. Each pair $(a_t, n_t) \in \mathbb{Z}_{\geq 0}^2$ represents the number a_t of a alleles observed out of n_t samples collected t generations ago. Missing data or generations where no sampling occurred are indicated by setting $n_t = 0$. Our model conditions on the sample sizes n_t , and we suppress notational dependence on them going forward.

The data-generating model is as follows. At time t , let the (unobserved) population frequency of the a allele be $f_t \in [0, 1]$. Given f_t , the data in generation t are binomially distributed with success probability f_t :

$$a_t | f_t \sim \text{Binom}(n_t, f_t). \quad (1)$$

The latent allele frequency trajectory $\mathbf{f} = (f_0, f_1, \dots, f_T)$ evolves according to a WF model with genic selection and no mutation (e.g., Ewens 2004). Given f_t and s_t , the number of individuals $F_{t-1} \in [0, 2N_{t-1}]$ possessing the a allele in next generation has distribution

$$F_{t-1} | f_t, s_t \sim \text{Binom}(2N_{t-1}, f'_t), \quad \text{where } f'_t = \frac{(1 + s_t/2)f_t}{1 + s_t f_t/2}, \quad (2)$$

and then we set $f_{t-1} = F_{t-1}/(2N_{t-1})$.

Let $\mathbf{a} = (a_0, \dots, a_T)$ denote the data. The complete likelihood is

$$p_s(\mathbf{a}, \mathbf{f}) = \pi_T(f_T)p(a_T | f_T) \prod_{t=0}^{T-1} p(a_t | f_t)p_s(f_t | f_{t+1}), \quad (3)$$

where $\pi_T(f_T)$ is a prior distribution on the initial allele frequency (described in more detail below), and the probabilities $p_s(f_t | f_{t+1})$ and $p(a_t | f_t)$ are specified by Equations 1 and 2. (Throughout this section, we use the notation p_s to denote probability distributions that depend on the selection parameters \mathbf{s} .) The likelihood of the observed data is obtained by marginalizing Equation 3 over \mathbf{f} :

$$p_s(\mathbf{a}) = \int_{\mathbf{f}} p_s(\mathbf{a}, \mathbf{f}). \quad (4)$$

By exploiting the Markov structure of Equation 3, the integral (4) can be efficiently evaluated using the forward algorithm. Each step of the forward algorithm costs $\mathcal{O}(N_{t-1}N_t)$ owing to the need to evaluate the transition probability (2) for all possible values of f_{t-1} and f_t . When the effective population size is large (greater than 10^3 , say), this quadratic scaling causes computation to become slow, and it is advantageous to model the latent allele trajectory f_t using a continuous approximation. Several have been proposed, including using the WF diffusion (Bollback et al. 2008; Malaspina et al. 2012; Lacerda and Seoighe 2014; Steinrücken et al. 2014; Ferrer-Admetlla et al. 2016), Gaussian approximations to the WF model (Mathieson and McVean 2013; Feder et al. 2014; Lacerda and Seoighe 2014; Terhorst et al. 2015), and approximations based on the beta distribution (Tataru et al. 2015, 2017; Gompert 2016; see also Malaspina 2016 and references therein). A recent review (Paris et al. 2019) found the beta-with-spikes (hereafter, **bws**) approximation of Tataru et al. (2017) to perform consistently better than other approaches, so we use it as our starting point.

In this model, the latent frequency $f_t \in [0, 1]$ of the selected allele is modeled as a mixture distribution with three components. There are two atoms at $f_t = 0$ and $f_t = 1$ to allow for the possibility of allele loss or fixation, and the third component is a beta density characterizing the intermediate frequencies, $f_t \in (0, 1)$. The form of this model is motivated by the fact that, in the original WF process, the probability of loss or fixation is positive, whereas it is zero if f_t possesses an absolutely continuous density.

Although the **bws** model is state of the art, room for improvement remains. Paris et al. (2019) found that, although generally accurate, the **bws** approximation degrades when selection is strong and the effective population size is small. Crucially, we cannot necessarily rule such a regime out when analyzing adDNA data. Another

potential shortcoming, not reported by Paris et al. (2019) but encountered when we implemented the **bws** model, concerns the method used to approximate the transition probability

$$p(f_{t+\Delta t} = y | f_t = x, N_t, s_t). \quad (5)$$

We found that errors in the moment recursions used to compute these probabilities (Equations 6 onward of Paris et al. 2019) tended to accumulate, leading to numerical instability and situations in which the variance of the resulting beta approximation, or the spike probabilities, were sometimes computed to be negative (Python code illustrating this phenomenon is included as [Supplemental Code S1](#)). This led us to consider refinements of the **bws** model.

Beta mixture model

Breakdown of the moment-based approximation can be explained by insufficient degrees of freedom. The two-parameter beta distribution is not flexible enough to accurately approximate the density (5) in all cases. A potential solution is to enrich the approximating class of distributions, by modeling the continuous component of Equation 5 as a *mixture* of beta distributions. This solution is intuitive and also has theoretical justification: By a famous result of Bernstein (e.g., Feller 2008), it holds for any continuous function $g: [0, 1] \rightarrow \mathbf{R}$ that

$$g(x) = \lim_{M \rightarrow \infty} \sum_{m=0}^M g(m/M)b_{m,M}(x), \quad \text{uniformly,} \quad (6)$$

where $b_{m,M}$ is proportional to the Beta($m+1, M-m+1$) density. Hence, by taking M on the right-hand side of Equation 6 to be large but finite, we can accurately approximate any absolutely continuous density on the unit interval. We refer to this model as the *beta-mixture-with-spikes* (**bmws**). A schematic of our model, which accompanies the discussion in the next few subsections, is shown in Figure 1.

Under **bmws**, the (posterior) density of f_t is modeled as a mixture of M beta densities, plus two atoms at $f_t = 0$ and $f_t = 1$. We abuse notation slightly and write this as

$$f_t \sim p_{t0}\delta_0 + p_{t1}\delta_1 + (1 - p_{t0} - p_{t1}) \sum_{m=0}^M c_{tm}\text{Beta}(\alpha_{tm}, \beta_{tm}), \quad (7)$$

where δ_x denotes a point mass at x , and M is a user-specified parameter that trades approximation accuracy for speed. To model allele frequency trajectories, we need to characterize the distribution of f_{t-1} when f_t has the distribution (7). We follow earlier work in using a moment-based approximation; however, the form of approximation is new. Previously (e.g., Lacerda and Seoighe 2014; Terhorst et al. 2015; Tataru et al. 2017; Paris et al. 2019), the mean and variance of f_{t-1} were obtained by Taylor expansion about the infinite-population (zero variance) allele frequency trajectory, and then a moment-matched Gaussian or beta distribution was used to approximate the distribution of f_{t-1} . Here we proceed differently, by directly modeling the action of the WF transition kernel on a beta-distributed random variable.

Assume first that $f_t \sim \text{Beta}(\alpha, \beta)$, and let f'_t and f_{t-1} be as in Equation 2. Using a computer algebra system, we determined that

$$\mathbf{E}f_{t-1} \approx \frac{\alpha(2\alpha + \beta(s+2) + 2)}{2(\alpha + \beta)(\alpha + \beta + 1)}, \quad (8)$$

$$\text{var } \mathbf{E}(f_{t-1} | f'_t) \approx \frac{\alpha\beta(\alpha(1-s) + \alpha + \beta s + \beta + 2)}{(\alpha + \beta)^2(\alpha + \beta + 1)(\alpha + \beta + 2)}, \quad (9)$$

$$\mathbf{E} \text{ var}(f_{t-1} | f'_t) \approx \frac{\alpha\beta(\alpha(2-s) + \beta(s+2) + 4)}{4N_{t-1}(\alpha + \beta)(\alpha + \beta + 1)(\alpha + \beta + 2)}. \quad (10)$$

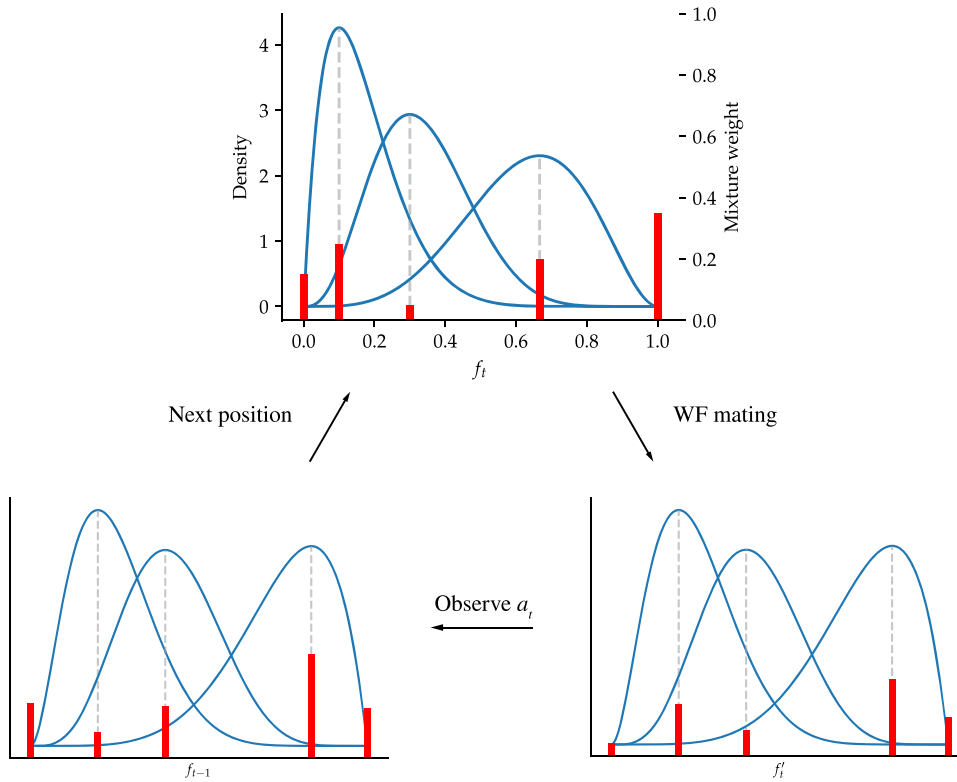


Figure 1. The BMWS model. At each time step t , the latent allele frequency f_t is modeled as a mixture of beta distributions, plus spikes at zero and one. In this diagram, there are $M = 3$ mixture components (blue lines). Mixture weights are indicated as red bars, including the spike weights p_0 and p_1 at $f_t = 0$ and $f_t = 1$, respectively. After Wright–Fisher (WF) mating, the shape of each beta mixture component, as well as the mixture weights, is updated according to Equation 15. After observing the data a_t , the mixture weights are again updated according to Bayes’ rule (Equation 16). The process then iterates.

(A Mathematica notebook verifying these computations is included as Supplemental Code S2.) These approximations are obtained by Taylor expansion of f'_t about $s=0$, followed by substituting in moments of the beta distribution. It would be easy to extend them to higher powers of s , but we did not find it necessary because $|s|=0.1$ is already at the extreme end of what we expect to find in natural data. Note that for $|s|<1$ (at least), the above equations imply $\text{var}f_{t-1} > 0$, so this approximation is robust to the pathology described above.

Using Equations 8 through 10, we can find α' , β' such that f_{t-1} has approximately a Beta(α' , β') distribution:

$$\alpha' = u\mathbf{E}f_{t-1}, \quad (11)$$

$$\beta' = u(1 - \mathbf{E}f_{t-1}), \quad (12)$$

$$u = \frac{\mathbf{E}f_{t-1}(1 - \mathbf{E}f_{t-1})}{\text{var}f_{t-1}} - 1. \quad (13)$$

The other components of the BMWS model are the “spikes” at $f_t = 0$ and $f_t = 1$. They are handled similarly to the original BWS model: At each mating event $f_t \rightarrow f_{t-1}$, some amount of probability mass is leaked from the beta (mixture) component to atomic components, corresponding to the events $F_{t-1}=0$ and $F_{t-1}=2N_{t-1}$ in Equation 2 (see the next section for a precise statement).

More generally, suppose the continuous component of f_t is a mixture, as in Equation 7. We make the following approximation in order to cheaply compute the conditional density of f_{t-1} . Let C_t have the categorical distribution $\mathbf{P}(C_t = m) \propto c_{tm}$, $c \in \{0, \dots, M\}$, and interpret Equation 7 hierarchically as

$$f_t | C_t = m \sim \text{Beta}(\alpha_{tm}, \beta_{tm}). \quad (14)$$

We assume that the continuous component of f_{t-1} is again a mixture of beta densities, with parameters α'_{tm} , β'_{tm} obtained by applying Equations 11 through 13 with $\mathbf{E}(f_{t-1}|C_t = m)$ (specified by Equation 14) in place of $\mathbf{E}f_{t-1}$. That is, we separately compute the effect of Equation 2 on each mixture component in Equation 7 and average the results together using the mixing weights \mathbf{c}_t . This “linear” approximation requires only $\mathcal{O}(M)$ computations and is much more efficient and easier to implement compared to modeling the effect of applying Equation 2 to the overall mixture shown in Equation 7. Although a closer approximation could be obtained by optimizing over the mixture weights \mathbf{c}_t , it would introduce additional computational expense and did not seem necessary in the examples we considered.

The astute reader will have noticed that, in contrast to some earlier works, we did not properly condition on nonfixation when constructing this approximation. That is, instead of, for example, $\mathbf{E}f_{t-1}$ in Equation 8, we should instead have considered

$$\mathbf{E}(f_{t-1}|0 < F_{t-1} < 2N_{t-1}).$$

However, the resulting expressions are very complex because they involve taking expectation over terms of the form $(f'_t)^k$ for k as high as $2N_{t-1}$. We opted for the simpler and more numerically stable Equations 8 through 10 and confirmed in simulations that the model is still accurate across a range of parameter settings.

Likelihood

The likelihood (4) is calculated using a variant of the usual forward algorithm for hidden Markov models. We explain this computation in greater detail here because the approach is nonstandard.

The forward algorithm recursively updates the so-called *filtering density* $p(f_t|a_0, \dots, a_T)$, which takes the form shown in Equation 7 under our model. Given the filtering density and the observation a_{t-1} , we need to extend the filtering density one step toward the present to obtain $p(f_{t-1}|a_{t-1}, \dots, a_T)$. This is accomplished in stages:

1. We use Equations 8 through 12 to compute α'_{tm} and β'_{tm} , as well as

$$p'_{t0} = p_{t0} + \mathbf{E}[p(F_{t-1} = 0|f_t, a_t, \dots, a_T)]$$

and similarly for p'_{t1} . This yields the predictive density

$$p_s(f_{t-1}|a_t, \dots, a_T) = p'_{t0}\delta_0 + p'_{t1}\delta_1 + \sum_{m=0}^M c'_{tm}\text{Beta}(\alpha'_{tm}, \beta'_{tm}), \quad (15)$$

where we define $c'_{tm} = (1 - p'_{t0} - p'_{t1})c_{tm}$.

2. We compute the probability

$$p_s(a_{t-1}|a_t, \dots, a_T) = \int_{f_{t-1}} p(a_{t-1}|f_{t-1})p_s(f_{t-1}|a_t, \dots, a_T),$$

noting that the integral can be evaluated analytically using Equations 1 and 15 and conjugacy.

3. We update the mixture weights in Equation 15 to incorporate the information added by observation a_{t-1} . Viewing a_{t-1} as a draw from the Bayesian hierarchical model defined by Equations 1 and 15, the posterior mixture weights on the beta mixture components are

$$c_{t-1,m}|a_{t-1}, \dots, a_T \propto c'_{t,m} \left(\frac{n_{t-1}}{a_{t-1}} \right) \frac{\text{B}(a_{t-1} + \alpha'_{tm}, n_{t-1} - a_{t-1} + \beta'_{tm})}{\text{B}(\alpha'_{tm}, \beta'_{tm})}, \quad (16)$$

where the right-hand side is the BetaBinomial($n_{t-1}, \alpha'_{tm}, \beta'_{tm}$) p.m.f. The posterior weight on the atom at $f_{t-1}=1$ is $p_{t-1,1} \propto \mathbf{1}_{[a_{t-1}=n_{t-1}]}$, and similarly for $p_{t-1,0}$. The constant of proportionality in these equations is $p_s(a_{t-1}|a_t, \dots, a_T)$, calculated in step 2.

4. The filtering distribution $p_s(f_{t-1}|a_{t-1}, \dots, a_T)$ takes the same form as Equation 7, with mixture weights as defined in the preceding step, $\alpha_{t-1,m} = a_{t-1} + \alpha'_{tm}$ and $\beta_{t-1,m} = n_{t-1} - a_{t-1} + \beta'_{tm}$.

Recalling Equation 4, the log-likelihood of the data is then

$$\log p_s(\mathbf{a}) = \sum_{t=0}^T \log p_s(a_t|a_{t+1}, \dots, a_T). \quad (17)$$

The running time of this algorithm is $\mathcal{O}(TM)$, as opposed to the standard forward algorithm, which scales quadratically in M if it were to denote the number of hidden states in an HMM. This enables us to set M fairly large, ensuring that our model can flexibly approximate differently shaped filtering distributions.

Prior distribution

The filtering recursion is initialized by setting $p(f_T) = \pi_T(f_T)$, where π_T is a prior on the ancestral allele frequency. When developing our method, we observed that the choice of prior affected the accuracy of inferences in the ancient past when analyzing aDNA data. This is because when the data are sparsely observed and allele counts are low, there is not enough data to overwhelm the prior in the early stages of the Markov chain. An uninformative choice of π_T can falsely suggest that the selected allele expe-

rienced a large change in frequency, potentially generating a spurious signal of selection. To mitigate this effect, we adopted a coordinate-ascent approach in which we alternatively maximized the log-likelihood (17) with respect to (1) the selective trajectory \mathbf{s} and (2) the prior π_T .

For the prior distribution, we assumed that $\pi_T \sim \text{Beta}(\alpha_T, \beta_T)$ and optimized over α_T, β_T . Although this choice of prior is not necessarily in the family of $\text{Beta}(i+1, n-i+1)$ mixture densities that comprise the interpolation scheme (6), we can accurately approximate it (or any other choice of prior) by setting M large, setting $c_{Tm} \propto f_{\pi_T}(m/M)$, where f_{π_T} is the prior's density function, and invoking the aforementioned Bernstein approximation theorem.

Inference

Given the probability model and approximations described in the preceding section, inference is now straightforward. Parameter estimation is performed as described in the previous section, with one additional modification. Depending on the quality and density of the data, many entries of \mathbf{s} may only be weakly resolved, and we also found it advantageous to add a regularization term. The objective function for all the analyses reported below was

$$\max_{\mathbf{s}} \log p_s(\mathbf{a}) - \lambda \sum_{t=0}^{T-1} (s_{t+1} - s_t)^2, \quad (18)$$

where $\lambda > 0$ is a tuning parameter. The regularizer penalizes variation in \mathbf{s} , with larger values of λ shrinking all entries toward a single common value, $s_0 = \dots = s_T$. The number of mixture components for the BMWS model was fixed to $M=100$, and we performed three rounds of coordinate ascent. For all the examples in this paper, we assumed that the size history (N_0, \dots, N_T) is known, but coestimation of selection and size history is also possible using our method and could be an avenue for future research. Finally, our method is implemented using a JIT-compiled, differentiable programming language (<https://github.com/google/jax>) to allow for efficient gradient-based fitting.

We use a parametric bootstrap to estimate the uncertainty in our inference. Specifically, after fitting the model, we sample allele frequency trajectories \mathbf{f} from the posterior distribution (Equation 7). We then sample observations conditional on the trajectory and the original sample sizes and times, and refit the model to those observations. We repeat this 1000 times and use the central 95% of results (based on the mean value of \mathbf{s}) as an estimate of the 95% credible interval for \mathbf{s} , taking into account the uncertainty in the allele frequency trajectory and the sampling of observations.

Simulations

We evaluated the performance of the estimator under three different types of selection, each lasting for $T=100$ generations:

- Constant selection with $s=0.01$ and initial frequency of 0.1;
- Selection that decreases sinusoidally from $s=+0.02$ to $s=-0.02$ and initial frequency of 0.1; and
- Selection that alternates between $+0.02$ and -0.02 every 20 generations and initial frequency of 0.5.

In each case, we simulated allele frequency trajectories in a WF population with $N=10^4$ and then sampled 100 haploid individuals every 10 generations. We also simulated the same selective models under two scenarios of variable effective population size:

- Exponential growth from $N=10^4$ to $N=10^5$; and
- $N=10^4$ with a bottleneck of $N=10^3$ lasting 10 generations.

For these scenarios, we ran the estimator both with the correct effective population size and incorrectly, assuming a constant $N=$

10^4 to evaluate its robustness to misspecification of N . We varied the smoothing parameter λ from $\log_{10}(\lambda)=1$ to 6 and report the root mean squared (RMS) bias, variance, and total error of the estimator. Finally, we evaluated the error of the estimator as the sample size and frequency vary.

These simulations explore the effects of relatively strong selection with human-like demographic parameters ($N=10^4$, 100 generations of observations, bottlenecks, and exponential growth; selection coefficients of $\mathcal{O}(0.01)$). However, other species may have very different sets of parameters. We therefore recommend that for any particular application, users should run simulations based on their prior parameter values in order to understand the behavior of the estimator in their specific case and to determine the appropriate smoothing parameter. We provide functions to easily implement simulations under arbitrary selective and population size scenarios. To illustrate this approach, we also ran the simulations described above using the sampling distribution of the British aDNA data used in the rest of paper.

aDNA data

We collected data from ancient British individuals dated to the past 4500 yr from the Allen Ancient DNA Resource (AADR version 44.3, <https://reich.hms.harvard.edu/allen-ancient-dna-resource-aadr-downloadable-genotypes-present-day-and-ancient-dna-data>) and from original sources (Martiniano et al. 2016; Schiffels et al. 2016; Olalde et al. 2018; Brace et al. 2019; Margaryan et al. 2020; Patterson et al. 2022). Most samples had been sequenced at sites targeted using the 1240k in-solution capture reagent, and the small number of shotgun samples had been genotyped at the 1240k SNPs so we therefore restricted our analysis to this set of SNPs. All data were pseudohaploid. After removing 22 PCA outliers, we were left with 529 ancient individuals and 98 present-day individuals from the GBR population of the 1000 Genomes Project (The 1000 Genomes Project Consortium 2015), processed into pseudohaploid data as part of the AADR (Fig. 2A).

Our method assumes that samples are drawn from a closed, randomly mating population in which every individual experiences the same selective pressures. Although no natural population satisfies these conditions, we chose to restrict to Britain dated in the period 4500 BP to present because it is the largest aDNA sample from a time and region that comes close to satisfying the assumptions of

the model for the following reasons. First, Britain is a relatively small region (compared with previous Europe-wide studies), meaning that selective pressures are more likely to be shared. Second, we know from previous aDNA studies that the last major change in ancestry in Britain occurred around 4500 BP (Olalde et al. 2018). Although recent work has shown more recent Bronze Age migrations into Britain (Patterson et al. 2022), these involved populations that were genetically similar and inhabited geographically adjacent regions. Third, we confirmed using principal component analysis (PCA) that all the ancient samples in our analysis clustered with the present-day British individuals from the 1000 Genomes Project and, more broadly, with other Northwestern European individuals in the context of present-day West Eurasia (Fig. 2B).

aDNA analysis

Starting with 1,150,639 autosomal SNPs, we removed 428,624 with a minor allele frequency (MAF) <0.1 in the full data set on the grounds that any SNP with a significant frequency shift in this time period would have intermediate MAF. We also removed 101,967 SNPs with $>90\%$ missingness and 210,725 SNPs with MAF = 0 in the ancient data to leave 409,232 SNPs genome-wide. We inferred selection coefficients \hat{s}_t at generation t for every SNP in the filtered data using a smoothing parameter of $\lambda=10^{4.5}$ and an effective population size of $N=10^4$. For each SNP, we summarize this estimate by the mean selection coefficient $\bar{s}=\frac{1}{T}\sum_{t=1}^T \hat{s}_t$

and the RMS selection coefficient $\|s\|=\left(T^{-1} \sum_{t=1}^T \hat{s}_t^2\right)^{1/2}$. We then computed the mean value of $\|s\|$ in 20-SNP sliding windows, sliding in 10-SNP increments, so each SNP contributes to two windows. We denote these window statistics as $\|s\|_{20}$. Finally, we fit a gamma distribution using the method of moments to the values of $\|s\|_{20}$ and used this fitted distribution to compute P -values for each window. We therefore calibrate the test statistics to the genome-wide background, analogous to the use of genomic control to account for genetic drift in association studies. We confirmed that this procedure leads to well-calibrated P -values when there is no temporal change in allele frequencies by repeating the analysis with the dates of each sample randomized.

We compared our results with two previous genome-wide selection scans. The first—an aDNA-based scan (Mathieson et al. 2015)—is an allele frequency scan to detect selection in approximately the past 8000 yr in Western Eurasia. The second, the SDS test (Field et al. 2016), is a scan based on haplotype lengths in the present-day United Kingdom population and is most sensitive to selection in the past few 1000 yr. First, we restricted the previous scans to the same set of SNPs used in the present scan. Next, for each window in the present scan, we computed the mean test statistics (chi-squared statistic for the aDNA scan and squared Z -score for the SDS) in each window and compared them with the test statistics generated by our method.

2015)—is an allele frequency scan to detect selection in approximately the past 8000 yr in Western Eurasia. The second, the SDS test (Field et al. 2016), is a scan based on haplotype lengths in the present-day United Kingdom population and is most sensitive to selection in the past few 1000 yr. First, we restricted the previous scans to the same set of SNPs used in the present scan. Next, for each window in the present scan, we computed the mean test statistics (chi-squared statistic for the aDNA scan and squared Z -score for the SDS) in each window and compared them with the test statistics generated by our method.

Polygenic selection test

We obtained summary statistics from genome-wide association studies (GWAS) for 28 quantitative traits (Tallal et al. 2012; Wood et al. 2014; Horikoshi

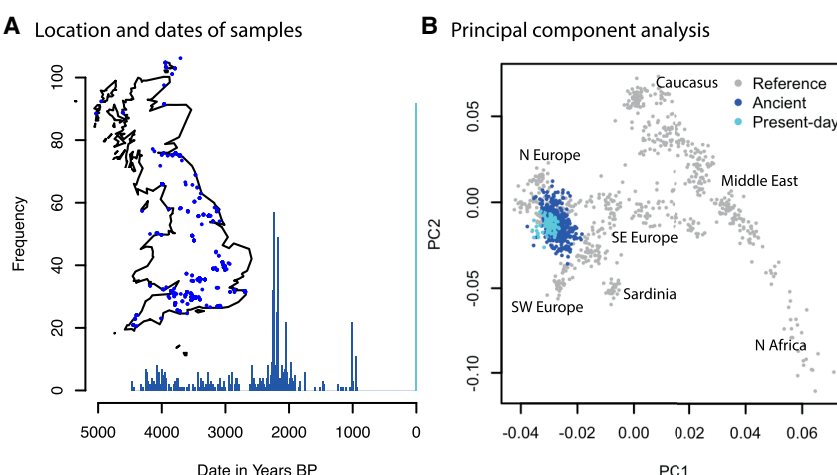


Figure 2. Ancient British data. (A) Histogram of dates of ancient individuals. Inset map shows locations of sites. (B) Principal components of ancient and present-day samples projected onto axes defined by 777 West Eurasian individuals (for details of these individuals, see Lazaridis et al. 2014).

et al. 2016; Chen et al. 2021; <http://www.nealelab.is/uk-biobank>). We took the intersection of GWAS SNPs with the 1240k SNPs, restricted to P -values $< 10^{-4}$, and pruned to an independent set of SNPs by iteratively taking the SNP with the smallest P -value and removing all other SNPs within 250 kb. For each trait, we calculated the correlation between effect size and estimated selection coefficient for each independent SNP.

Results

Our estimator successfully recovers complex selection trajectories from simulated data (Fig. 3), with total sample sizes and times equal to the ancient sample, although individual selection coefficient estimates can have considerable uncertainty—on the order of $\pm 0.01 - 0.02$ with these parameter values. This suggests that with the data available we should be able to reliably detect selection coefficients around 0.02, similar to the SDS and aDNA allele frequency approaches that we compare to our method (Mathieson et al. 2015; Field et al. 2016). The absolute error of the estimate does not depend on the selection coefficient, meaning that, at least in this parameter range, we cannot reliably distinguish smaller selection coefficients from zero. As expected, the optimal smoothing parameter depends on the true selective trajectory: the smoother the trajectory, the higher the optimal λ (Supplemental Fig. S1). We therefore recommend choosing λ based on simulations, with parameters that are informed by the specific application.

The estimator performs similarly in the presence of population size bottlenecks or exponential growth, although it tends to slightly oversmooth changes in s in these cases (Supplemental Fig. S2). It is relatively robust to misspecification of effective population size: If we input constant N to the estimator, results are not noticeably different than if we specify the correct population size history (Supplemental Fig. S3). Increasing the size and frequency of sampling reduces error (Supplemental Fig. S4), al-

though, in general, sample size is more important than sampling frequency; all else being equal, it is better to have infrequent samples of large sizes than frequent small samples.

In the ancient British data, we identified seven regions with genome-wide significant evidence of selection (Table 1; Fig. 4A; Supplemental Table S2). We used a P -value cutoff of 10^{-7} as a genome-wide significant cutoff. Although conservative for the 68,061 overlapping windows in our analysis, we used this value because when we reran the analysis with randomized sample dates, no window had a smaller P -value (Fig. 4B). Three of these regions, which we denote HLA1, HLA2, and HLA3, are in the HLA region on Chromosome 6 (Supplemental Fig. S5), although these themselves may contain multiple signals. An eighth apparent signal on Chromosome 4 containing the gene *LINC00955* is likely artifactual. The lead SNP rs4690044 has a MAF of zero in present-day samples but is around 0.5 in ancient samples. In gnomAD (Karczewski et al. 2020), rs4690044 has a MAF of 0.48 but no homozygotes, suggesting an artifact call caused by a duplication. An additional locus on Chromosome 12 ($P = 2.5 \times 10^{-7}$), which contains the gene *OAS1* and is known to be a target of adaptive Neanderthal introgression (Sams et al. 2016), was significant at a Bonferroni-corrected significance threshold ($P = 7.3 \times 10^{-7}$).

All seven of these regions were identified by a previous allele frequency-based selection scan using aDNA to detect selection in West Eurasia over the past 8000 yr (Fig. 4D; Mathieson et al. 2015). Only *LCT* and the HLA region show significant evidence of selection in a haplotype-based scan using present-day sequence data that aimed to detect selection in Britain in the past few 1000 yr (Fig. 4C; Field et al. 2016) or in a scan based on identifying very recent coalescence times (about 50 generations) in the UK Biobank (Nait Saada et al. 2020).

For the non-HLA signals for which we have a strong candidate for the causal variant based on previous literature, we examined the precise timing and trajectory of selection estimates from our model (Fig. 5). The most significant signal was the well-known

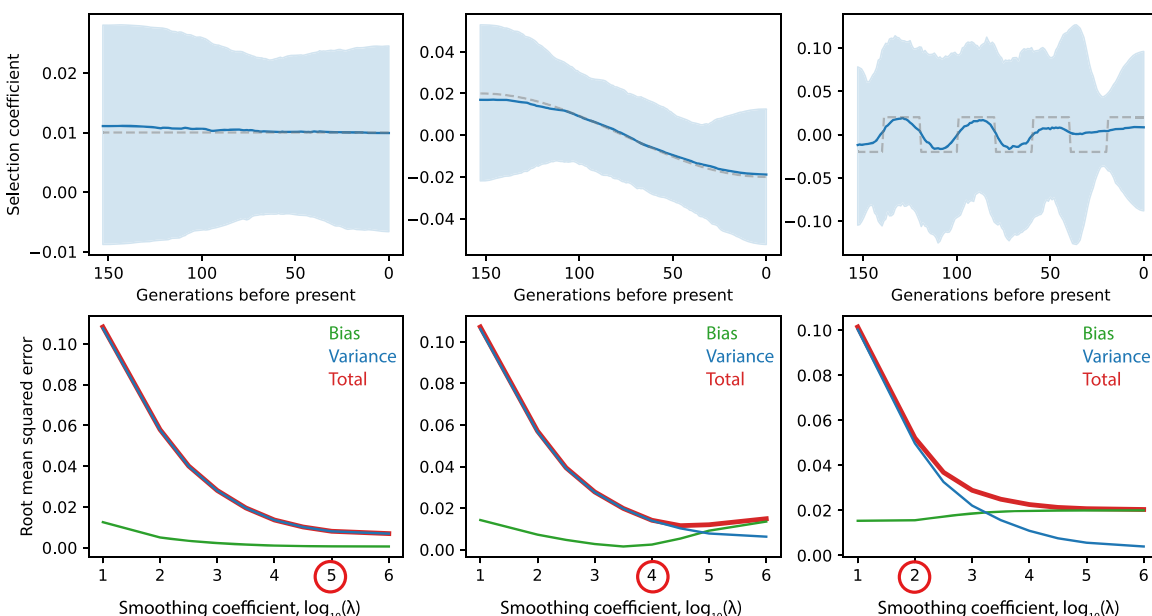


Figure 3. Simulation results for the sampling distribution of the ancient British data. Each column shows a different selection coefficient trajectory. (Top) Estimated selection coefficients. Dashed line indicates simulated selection coefficient; solid blue line, mean selection coefficient from 1000 simulations; and light blue shaded area, region containing point estimates from 950/1000 simulations. (Bottom) Square root of squared bias, variance, and total squared error as a function of $\log_{10}(\lambda)$. The circled value is the one used for the estimates in the top row.

Table 1. Genome-wide significant regions

Locus	Chr	Start (hg19)	End (hg19)	Target SNP	Allele	\bar{s}
<i>LCT</i>	2	136,582,694	136,714,178	rs4988235	G	0.064
<i>SLC45A2</i>	5	33,887,419	33,964,938	rs16891982	C	0.043
<i>HLA1</i>	6	28,234,597	28,374,902	(rs6922111)	(C)	(0.046)
<i>HLA2</i>	6	31,026,009	31,361,897	(rs4947296)	(C)	(0.034)
<i>HLA3</i>	6	32,083,175	32,581,973	(rs204994)	(C)	(0.042)
<i>DHCR7</i>	11	71,142,350	71,183,690	rs7944926	A	0.051
<i>HERC2</i>	15	28,334,927	28,526,228	rs12913832	A	0.017

For non-HLA regions, we give the chromosome and position of the center of the lead window, the selected SNP (based on previous literature), the selected allele, and the mean selection coefficient of the lead SNP. For HLA regions, we give the co-ordinates of the three regions that contain significant signals (Supplemental Fig. S5) and the SNPs with the largest test statistic $\|s\|$. Parentheses indicate that we do not know whether these specific SNPs were the targets of selection. \bar{s} is the average selection coefficient over the observed time period.

LCT locus on Chromosome 2, where the selected allele is associated with lactase persistence (Enattah et al. 2002; Bersaglieri et al. 2004). We find that selection for the persistence allele was strongest ($s \approx 0.08$) from 150 to 100 generations before the present (roughly 4500–3000 BP) before decreasing to around 0.02 in the past 50 generations. This large change in strength of selection might explain the wide range of estimates from models that assume a constant value (Bersaglieri et al. 2004; Peter et al. 2012; Mathieson and Mathieson 2018). At *DHCR7*, the haplotype tagged by the SNP in our analysis, rs7944926, is associated with protection against vitamin D insufficiency (Wang et al. 2010) and has been shown to have been under recent selection in both Europe (Mathieson et al. 2015) and East Asia (Kuan et al. 2013). We infer

that, in Britain, the selection coefficient increased over the past 150 generations, from around zero to 0.06, leading to an increase in frequency from ~20% to 60% over the past 3000 yr (Fig. 5).

Derived alleles at *SLC45A2* and *HERC2* are associated with light skin, hair, and eye pigmentation (Norton et al. 2007; Eiberg et al. 2008; Canelo-Xandri et al. 2018; Hysi et al. 2018; Simcoe et al. 2021). Both these alleles have been shown to have been under selection broadly in Europe (Lao et al. 2007; Norton et al. 2007; Donnelly et al. 2012) and specifically during the Holocene (Wilde et al. 2014; Mathieson et al. 2015). Time series of aDNA have shown that both alleles were under selection in the past 5000 yr in Eastern Europe (Wilde et al. 2014). There, the derived *SLC45A2* allele increased in frequency from 40% to 90% over the

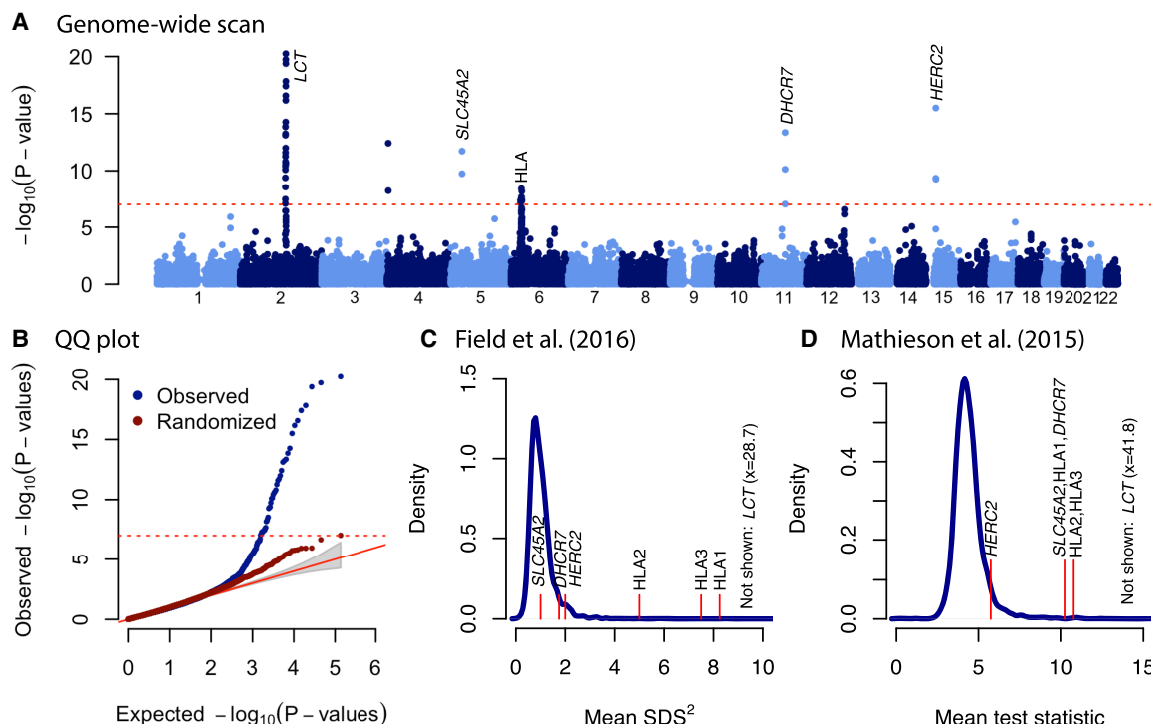


Figure 4. Genome-wide scan for selection in Britain. (A) P -values for selection in 20-SNP sliding windows. Genome-wide significant ($P < 10^{-7}$) windows are labeled with the closest gene or known target of selection. (B) QQ plot for observations in *A* (blue) and after randomizing the dates of each sample (red). (C) Comparison with results of Field et al. (2016). Blue solid line shows the density of mean SDS^2 in 20-SNP windows. Labeled red lines indicate windows that are genome-wide significant in our analysis. (D) Comparison with results of Mathieson et al. (2015). Blue solid line shows the density of mean χ^2 statistic in 20-SNP windows. Labeled red lines indicate windows that are genome-wide significant in our analysis. In both C and D, *HERC2* is approximately at the upper fifth percentile of the distribution.

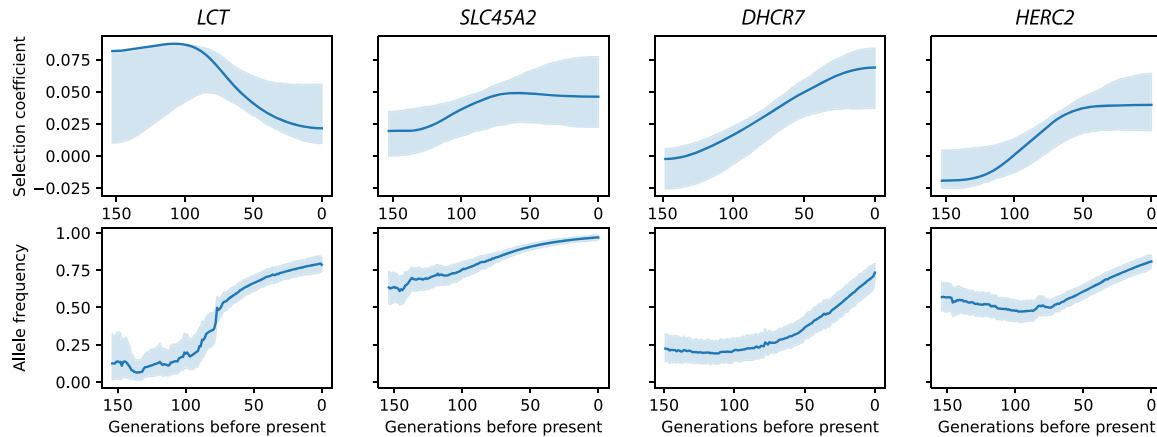


Figure 5. Trajectories of genome-wide significant non-HLA loci. Solid lines show the inferred selection coefficient and trajectory of the lead SNP given in Table 1. Shaded areas show 95% credible intervals based on resampling of the allele frequency trajectories and observations. (Top) Estimated selection coefficients. (Bottom) Estimated allele frequency trajectories.

past 5000 yr, suggesting a selection coefficient of around 0.03, very similar to our estimate of selection in Britain during the same time (Fig. 5). For the derived *HERC2* allele, we estimate a selection coefficient of 0.02–0.04, similar to that estimated in Eastern Europe, although we find that in Britain, selection was largely restricted to approximately the past 2000 yr. Wilde et al. (2014) also found a derived allele of *TYR* to be under strong selection in Eastern Europe, but we find little evidence that it was under selection in Britain, except possibly before 3000 BP (window P -value = 0.03) (Supplemental Fig. S6).

At the HLA, we find three regions with genome-wide significant evidence of selection, which we denote HLA1–3 (Supplemental Fig. S5). All three correspond to regions identified by Mathieson et al. (2015) and also have strong evidence of selection in the Field et al. (2016) scan (Fig. 4C). Because of high gene density and complex patterns of linkage disequilibrium in the re-

gion, we did not attempt to identify causal genes or variants. However, we note that the lead SNP at HLA1 is strongly associated with a decreased risk of celiac disease in the UK Biobank (Canela-Xandri et al. 2018). The lead HLA2 SNP is associated with an increased risk of ankylosing spondylitis (Canela-Xandri et al. 2018), but the region contains the gene *HLA-C*, a variant of which is the strongest known risk factor for psoriasis (Yin et al. 2015). Finally, the lead SNP at HLA3 is strongly associated with a decreased risk of celiac disease and psoriasis (Canela-Xandri et al. 2018). These associations suggest that risk of these diseases has been affected by selection, even if they themselves are not the direct targets.

Finally, we searched for evidence of polygenic selection by testing for a correlation between GWAS effect size and selection coefficient for 28 anthropometric and morphological traits (Fig. 6A; Supplemental Table S1; Supplemental Fig. S7). We find significant

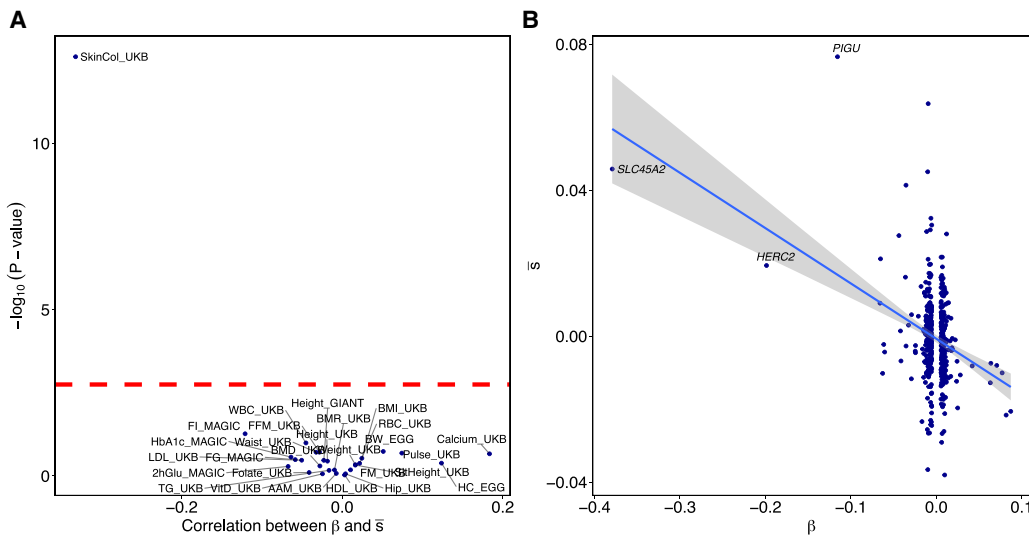


Figure 6. Evidence of polygenic selection. (A) Each point represents a single GWAS. The x-axis gives the (Pearson) correlation between effect size estimates, β , and selection coefficient estimates, \bar{s} , for independent SNPs with GWAS P -value $< 10^{-4}$ and minor allele frequency (MAF) $> 5\%$. The y-axis gives the $\log_{10}(P\text{-value})$ for null hypothesis of no correlation. Abbreviations, exact values, and sources are given in Supplemental Table S1. (B) Effect sizes and selection coefficient estimates for independent skin color-associated SNPs in the UK Biobank with GWAS P -value $< 10^{-4}$ and MAF $> 5\%$. If the three labeled large-effect SNPs are removed, the correlation is weaker but still significant ($\rho = -0.20$, $P = 1.5 \times 10^{-5}$).

evidence of polygenic selection for reduced skin pigmentation ($P = 3.6 \times 10^{-16}$) (Fig. 6B) but none of the other 27 traits ($P > 0.04$). Although not statistically significant, the largest absolute correlation apart from skin pigmentation is for increased calcium. We do not detect evidence of selection on any of the phenotypes identified by Field et al. (2016) as under selection in Britain in the past 2000 yr, including height, infant head circumference, and fasting insulin.

Discussion

Our fast and flexible estimator allowed us to perform a direct genome-wide scan for selection based on allele frequency trajectories. On our standard compute cluster, average run-time for each SNP was 41 sec, requiring 220 Mb of RAM, so analyzing all 1.15 million loci took around 13,000 CPU h in total. All of the significant loci we identified have been identified by a previous allele frequency-based scan using aDNA (Mathieson et al. 2015). However, that approach scanned for selection broadly in Holocene Europe and was unable to localize selection further in either space or time. Here, we are able to localize selection to Britain in the past 4500 yr and, even further, to identify changes in the strength of selection over that time period (Fig. 5). We are also able to identify selected loci that were not identified in studies of much larger samples of present-day individuals (Field et al. 2016; Nait Saada et al. 2020).

On the other hand, when we search for polygenic selection, the only trait for which we find significant evidence is skin pigmentation, which is known to have been under selection in Europe more broadly into this time period (Wilde et al. 2014; Mathieson et al. 2015; Field et al. 2016; Ju and Mathieson 2021). Although many previous studies (Turchin et al. 2012; Berg and Coop 2014; Mathieson et al. 2015; Robinson et al. 2015; Field et al. 2016) reported evidence for recent selection on height, this has been shown to be largely driven by residual stratification in the GIANT Consortium GWAS (Berg et al. 2019; Sohail et al. 2019). Evidence of recent polygenic selection for other traits (e.g., Field et al. 2016) may suffer from the same issue, although findings based on the UK Biobank GWAS results may be more reliable. It is also possible that our negative findings reflect a lack of power. Even though our approach is relatively well-powered to detect strong selection compared with other selection scans, it may be less able to detect the weak selection that contributes to polygenic adaptation even in aggregate. A more complete investigation of the way in which the time series analysis in this study could be used to detect polygenic selection is a question for future work.

Although there may have been multiple environmental drivers of selection, taken together, our results strongly suggest that a major selective pressure at this time was for increased calcium largely moderated through increased vitamin D levels. Vitamin D is required for the absorption of calcium, and deficiency leads to bone deformities with potentially major effects on fitness. Because a major source of vitamin D is synthesis in the skin in the presence of UV radiation, the cloudy skies of Britain are likely to have limited this synthesis. The Mesolithic inhabitants of Britain may have avoided this problem through consumption of vitamin D-rich marine resources, but later Neolithic and Bronze Age populations, including those in our study, relied on agricultural products for their subsistence (Richards et al. 2003), leading to a need for genetic adaptation.

In fact, almost all of our signals of selection can be related to selection for increased vitamin D or directly for increased calcium. Selection at *SLC45A2* and *HERC2*, as well as selection for lighter skin pigmentation more generally, naturally leads to increased penetration of UV into the skin and therefore higher levels of vitamin D (Murray 1934; Jablonski and Chaplin 2010). Lactase persistence allows the consumption of milk, which contains both calcium and a small amount of vitamin D. This “calcium absorption” hypothesis has long been suggested to explain the high frequency of the persistence phenotype in Northern Europe (Flatz and Rotthauwe 1973; Gerbault et al. 2011). *DHCR7* is directly involved in vitamin D metabolism, and the selected allele protects against insufficiency (Wang et al. 2010). Although the HLA associations are more difficult to specifically identify, two of the selected alleles are protective against celiac disease, which itself is a risk factor for malabsorption of calcium and vitamin D and consequent osteoporosis (Meyer et al. 2001). Strong selective pressure for increased vitamin D and calcium levels is therefore a plausible and parsimonious explanation for the patterns of selection that we observe in this data set.

The main limitation of our approach is the assumption of population continuity. Although there is evidence of external migration into Britain during the time period we investigated (Patterson et al. 2022), there is relatively little change in genetic ancestry because the sources of that migration are genetically similar populations from other nearby parts of Northern Europe. If this affects our results, it would likely mean that some of the selection we detected actually occurred in those neighboring populations, somewhat earlier than the dates we find here. However, given that the selection pressures we detect are likely to be shared with these similar populations anyway, we do not think this possibility has a major impact on the interpretation of our results. This limitation is more serious if we want to extend the temporal and geographic range of our analysis. In particular, both ancient and present-day individuals from the Iberian and Italian peninsulas are much more genetically diverse than those from Britain (Supplemental Fig. S8). Because of this, and the much smaller ancient sample sizes, we did not analyze selection in these Southern European populations, although identifying differences in selective pressures between Northern and Southern Europe is an important direction for future analysis.

Although we have identified the loci under the strongest selection in recent British history, there is evidence in our data of additional selected loci. For example, several known loci, including *OAS1* ($P = 2.5 \times 10^{-7}$) (Sams et al. 2016) and *FADS1* ($P = 1.5 \times 10^{-5}$) (Mathieson et al. 2015), have evidence of selection, although below genome-wide significance. With larger sample sizes, we can expect that these and other, potentially novel, loci would be identified. An alternative way to increase sample size would be to modify our method to analyze genotype likelihoods rather than pseudohaploid calls. We estimate that this could increase effective sample size by up to 22%. An even bigger increase could be gained by using genotype imputation, although with the caveat that imputation may be less reliable in strongly selected regions. There are also several technical limitations that may affect interpretations of our results. For example, we identified at least one locus where systematic differences between ancient and present-day samples created a spurious signal of selection. Other systematic differences related to mapping errors, or aDNA damage, might create similar effects. It is important therefore to check that results based on the comparison of ancient and present-day samples are robust by verifying that they are consistent when present-day samples are

excluded or, as we have performed here, that they are consistent with signals derived from present-day data alone. Another limitation is that we rely on sites included in the 1240k capture reagent and therefore cannot detect selection on rare SNPs or structural variants that are not tagged by such SNPs. Imputation or large data sets of shotgun sequence data might extend the range of variation on which selection can be detected.

Our study shows the power of aDNA to robustly detect and precisely characterize the timing of natural selection in humans. We appear to have similar power to detect selection as previously published methods based on present-day and ancient data. On the other hand, present-day sample sizes will always be much larger, and approaches that can scale to hundreds of thousands or millions of genomes (Nait Saada et al. 2020) will probably be more powerful. The major advantage of aDNA is the ability to precisely estimate the timing of selection, suggesting a potential hybrid approach using very large present-day data sets to identify nonneutral regions of the genome and then use aDNA time series to characterize the timing and nature of selection at those loci. Indeed, several of the loci that we identify have evidence of substantial change in the strength of selection over the past 4500 yr, suggesting that modeling this variability may be an important addition to previous approaches that assume constant selective pressure. One caveat is that in order to do this, we need to be able to identify the selected variant at a locus, which is not always possible (e.g., in the case of HLA). Indeed, imperfect tagging of the causal variant could lead to spurious signals of time-varying selection, as could dominance coefficients different from 0.5 or spatially structured selection. In particular, lactase persistence is dominant, although enzymatic activity is not (Ségurel and Bon 2017). Therefore, selection on *LCT* could act in a dominant fashion, which could give the appearance of decreasing the selective coefficient over time. If the selective pressure on *LCT* did decrease over time, perhaps owing to cultural changes, it may have contributed to an increase in selective pressures related to other sources (e.g., pigmentation and metabolism). In this way, culture could have determined the genetic response to a constant environmental selective pressure. The prospect of exploring this and similar interactions is an exciting future direction for aDNA research.

Software availability

Source codes to run the estimator and reproduce the analyses in this paper are available at GitHub (<https://github.com/jthlab/bmws>) and as Supplemental Codes S1–S3.

Competing interest statement

The authors declare no competing interests.

Acknowledgments

We thank Pontus Skoglund for helpful comments. This research was funded by the National Institute of General Medical Sciences (R35GM133708 to I.M.) and the National Science Foundation (DMS-2052653 to J.T.). The content is solely the responsibility of the authors and does not necessarily represent the official views of the funding agencies.

Author contributions: I.M. and J.T. conceived and designed the study, wrote the code, analyzed the data, and wrote the manuscript.

References

- The 1000 Genomes Project Consortium. 2015. A global reference for human genetic variation. *Nature* **526**: 68–74. doi:10.1038/nature15393
- Berg JJ, Coop G. 2014. A population genetic signal of polygenic adaptation. *PLOS Genet* **10**: e1004412. doi:10.1371/journal.pgen.1004412
- Berg JJ, Harpak A, Sinnott-Armstrong N, Joergensen AM, Mostafavi H, Field Y, Boyle EA, Zhang X, Racimo F, Pritchard JK, et al. 2019. Reduced signal for polygenic adaptation of height in UK Biobank. *eLife* **8**: e39725. doi:10.7554/eLife.39725
- Bersaglieri T, Sabeti PC, Patterson N, Vanderplough T, Schaffner SF, Drake JA, Rhodes M, Reich DE, Hirschhorn JN. 2004. Genetic signatures of strong recent positive selection at the lactase gene. *Am J Hum Genet* **74**: 1111–1120. doi:10.1086/421051
- Bollback JP, York TL, Nielsen R. 2008. Estimation of $2N_{es}$ from temporal allele frequency data. *Genetics* **179**: 497–502. doi:10.1534/genetics.107.085019
- Brace S, Diekmann Y, Booth TJ, van Dorp L, Faltyskova Z, Rohland N, Mallik S, Olalde I, Ferry M, Michel M, et al. 2019. Ancient genomes indicate population replacement in Early Neolithic Britain. *Nat Ecol Evol* **3**: 765–771. doi:10.1038/s41559-019-0871-9
- Can O, Rawlik K, Tenesa A. 2018. An atlas of genetic associations in UK Biobank. *Nat Genet* **50**: 1593–1599. doi:10.1038/s41588-018-0248-z
- Chen J, Spracklen CN, Marenne G, Varshney A, Corbin LJ, Luan J, Willems SM, Wu Y, Zhang X, Horikoshi M, et al. 2021. The trans-ancestral genomic architecture of glycemic traits. *Nat Genet* **53**: 840–860. doi:10.1038/s41588-021-00852-9
- Donnelly MP, Paschou P, Grigorenko E, Gurwitz D, Barta C, Lu RB, Zhukova OV, Kim JJ, Siniscalco M, New M, et al. 2012. A global view of the OCA2-HERC2 region and pigmentation. *Hum Genet* **131**: 683–696. doi:10.1007/s00439-011-1110-x
- Eiberg H, Troelsen J, Nielsen M, Mikkelsen A, Mengel-From J, Kjaer KW, Hansen L. 2008. Blue eye color in humans may be caused by a perfectly associated founder mutation in a regulatory element located within the HERC2 gene inhibiting OCA2 expression. *Hum Genet* **123**: 177–187. doi:10.1007/s00439-007-0460-x
- Enattah NS, Sahl T, Savilahti E, Terwilliger JD, Peltonen L, Järvelä I. 2002. Identification of a variant associated with adult-type hypolactasia. *Nat Genet* **30**: 233–237. doi:10.1038/ng826
- Ewens WJ. 2004. *Mathematical population genetics: theoretical introduction*, Vol. 1. Springer, New York.
- Feder AF, Kryazhimskiy S, Plotkin JB. 2014. Identifying signatures of selection in genetic time series. *Genetics* **196**: 509–522. doi:10.1534/genetics.113.158220
- Feller W. 2008. *An introduction to probability theory and its applications*, Vol. 2. John Wiley & Sons, New York.
- Ferrer-Admetlla A, Leuenberger C, Jensen JD, Wegmann D. 2016. An approximate Markov model for the Wright-Fisher diffusion and its application to time series data. *Genetics* **203**: 831–846. doi:10.1534/genetics.115.184598
- Field Y, Boyle EA, Telis N, Gao Z, Gaulton KJ, Golan D, Yengo L, Rocheleau G, Froguel P, McCarthy MI, et al. 2016. Detection of human adaptation during the past 2000 years. *Science* **354**: 760–764. doi:10.1126/science.aag0776
- Flatz G, Rotthauwe HW. 1973. Lactose nutrition and natural selection. *Lancet* **302**: 76–77. doi:10.1016/S0140-6736(73)93267-4
- Gerbault P, Liebert A, Itam Y, Powell A, Currat M, Burger J, Swallow DM, Thomas MG. 2011. Evolution of lactase persistence: an example of human niche construction. *Philos Trans R Soc Lond B Biol Sci* **366**: 863–877. doi:10.1098/rstb.2010.0268
- Gompert Z. 2016. Bayesian inference of selection in a heterogeneous environment from genetic time-series data. *Mol Ecol* **25**: 121–134. doi:10.1111/mec.13323
- Horikoshi M, Beaumont RN, Day FR, Warrington NM, Kooijman MN, Fernandez-Tajes J, Feenstra B, van Zuydam NR, Gaulton KJ, Grarup N, et al. 2016. Genome-wide associations for birth weight and correlations with adult disease. *Nature* **538**: 248–252. doi:10.1038/nature19806
- Hysi PG, Valdes AM, Liu F, Furlotte NA, Evans DM, Bataille V, Visconti A, Hemani G, McMahon G, Ring SM, et al. 2018. Genome-wide association meta-analysis of individuals of European ancestry identifies new loci explaining a substantial fraction of hair color variation and heritability. *Nat Genet* **50**: 652–656. doi:10.1038/s41588-018-0100-5
- Jablonski NG, Chaplin G. 2010. Human skin pigmentation as an adaptation to UV radiation. *Proc Natl Acad Sci* **107** (Suppl 2): 8962–8968. doi:10.1073/pnas.0914628107
- Ju D, Mathieson I. 2021. The evolution of skin pigmentation-associated variation in West Eurasia. *Proc Natl Acad Sci* **118**: e2009227118. doi:10.1073/pnas.2009227118
- Karczewski KJ, Francioli LC, Tiao G, Cummings BB, Alfoldi J, Wang Q, Collins RL, Laricchia KM, Ganna A, Birnbaum DP, et al. 2020. The

- mutational constraint spectrum quantified from variation in 141,456 humans. *Nature* **581**: 434–443. doi:10.1038/s41586-020-2308-7
- Kerner G, Laval G, Patin E, Boisson-Dupuis S, Abel L, Casanova JL, Quintana-Murci L. 2021. Human ancient DNA analyses reveal the high burden of tuberculosis in Europeans over the last 2,000 years. *Am J Hum Genet* **108**: 517–524. doi:10.1016/j.ajhg.2021.02.009
- Kuan V, Martineau AR, Griffiths CJ, Hyppönen E, Walton R. 2013. *DHCRT* mutations linked to higher vitamin D status allowed early human migration to northern latitudes. *BMC Evol Biol* **13**: 144. doi:10.1186/1471-2148-13-144
- Lacerda M, Seoighe C. 2014. Population genetics inference for longitudinally-sampled mutants under strong selection. *Genetics* **198**: 1237–1250. doi:10.1534/genetics.114.167957
- Lao O, de Gruyter JM, van Duijn K, Navarro A, Kayser M. 2007. Signatures of positive selection in genes associated with human skin pigmentation as revealed from analyses of single nucleotide polymorphisms. *Ann Hum Genet* **71**: 354–369. doi:10.1111/j.1469-1809.2006.00341.x
- Lazaridis I, Patterson N, Mittnik A, Renaud G, Mallick S, Kirsanow K, Sudmant PH, Schraiber JG, Castellano S, Lipsom M, et al. 2014. Ancient human genomes suggest three ancestral populations for present-day Europeans. *Nature* **513**: 409–413. doi:10.1038/nature13673
- Malaspina A-S. 2016. Methods to characterize selective sweeps using time serial samples: an ancient DNA perspective. *Mol Ecol* **25**: 24–41. doi:10.1111/mec.13492
- Malaspina A-S, Malaspina O, Evans SN, Slatkin M. 2012. Estimating allele age and selection coefficient from time-serial data. *Genetics* **192**: 599–607. doi:10.1534/genetics.112.140939
- Margaryan A, Lawson DJ, Sikora M, Racimo F, Rasmussen S, Moltke I, Cassidy LM, Jørsboe E, Ingason A, Pedersen MW, et al. 2020. Population genomics of the Viking world. *Nature* **585**: 390–396. doi:10.1038/s41586-020-2688-8
- Martiniano R, Caffell A, Holst M, Hunter-Mann K, Montgomery J, Müldner G, McLaughlin RL, Teasdale MD, Van Rheezen W, Veldink JH, et al. 2016. Genomic signals of migration and continuity in Britain before the Anglo-Saxons. *Nat Commun* **7**: 10326. doi:10.1038/ncomms10326
- Mathieson S, Mathieson I. 2018. *FADS1* and the timing of human adaptation to agriculture. *Mol Biol Evol* **35**: 2957–2970. doi:10.1093/molbev/msy180
- Mathieson I, McVean G. 2013. Estimating selection coefficients in spatially structured populations from time series data of allele frequencies. *Genetics* **193**: 973–984. doi:10.1534/genetics.112.147611
- Mathieson I, Lazaridis I, Rohland N, Mallick S, Patterson N, Roodenberg SA, Harney E, Stewardson K, Fernandes D, Novak M, et al. 2015. Genome-wide patterns of selection in 230 ancient Eurasians. *Nature* **528**: 499–503. doi:10.1038/nature16152
- Meyer D, Stavropoulos S, Diamond B, Shane E, Green PH. 2001. Osteoporosis in a North American adult population with celiac disease. *Am J Gastroenterol* **96**: 112–119. doi:10.1111/j.1572-0241.2001.03507.x
- Murray FG. 1934. Pigmentation, sunlight, and nutritional disease. *Am Anthropol* **36**: 438–445. doi:10.1525/aa.1934.36.3.02a00100
- Nait Saada J, Kalantzis G, Shyr D, Cooper F, Robinson M, Gushev A, Palamara PF. 2020. Identity-by-descent detection across 487,409 British samples reveals fine scale population structure and ultra-rare variant associations. *Nat Commun* **11**: 6130. doi:10.1038/s41467-020-19588-x
- Norton HL, Kittles RA, Parra E, McKiegu P, Mao X, Cheng K, Canfield VA, Bradley DG, McEvoy B, Shriver MD, et al. 2007. Genetic evidence for the convergent evolution of light skin in Europeans and East Asians. *Mol Biol Evol* **24**: 710–722. doi:10.1093/molbev/msl203
- Oalalde I, Brace S, Allentoft ME, Armit I, Kristiansen K, Booth T, Rohland N, Mallick S, Szécsényi-Nagy A, Mittnik A, et al. 2018. The Beaker phenomenon and the genomic transformation of northwest Europe. *Nature* **555**: 190–196. doi:10.1038/nature25738
- Oalalde I, Mallick S, Patterson N, Rohland N, Villalba-Mouco V, Silva M, Dulias K, Edwards CJ, Gandini F, Pala M, et al. 2019. The genomic history of the Iberian Peninsula over the past 8000 years. *Science* **363**: 1230–1234. doi:10.1126/science.aav4040
- Paris C, Servin B, Boitard S. 2019. Inference of selection from genetic time series using various parametric approximations to the Wright-Fisher model. *G3 (Bethesda)* **9**: 4073–4086. doi:10.1534/g3.119.400778
- Patterson N, Isakov M, Booth T, Büster L, Fischer CE, Oalalde I, Ringbauer H, Akbari A, Cheroneit O, Bleasdale M, et al. 2022. Large-scale migration into Britain during the Middle to Late Bronze Age. *Nature* **601**: 588–594. doi:10.1038/s41586-021-04287-4
- Peter BM, Huerta-Sánchez E, Nielsen R. 2012. Distinguishing between selective sweeps from standing variation and from a *de novo* mutation. *PLoS Genet* **8**: e1003011. doi:10.1371/journal.pgen.1003011
- Richards MP, Schulting RJ, Hedges RE. 2003. Archaeology: sharp shift in diet at onset of neolithic. *Nature* **425**: 366. doi:10.1038/425366a
- Robinson MR, Hemani G, Medina-Gomez C, Mezzavilla M, Esko T, Shakhsbazov K, Powell JE, Vinkhuyzen A, Berndt SI, Gustafsson S, et al. 2015. Population genetic differentiation of height and body mass index across Europe. *Nat Genet* **47**: 1357–1362. doi:10.1038/ng.3401
- Sams AJ, Dumaine A, Nédélec Y, Yotova V, Alfieri C, Tanner JE, Messer PW, Barreiro LB. 2016. Adaptively introgressed Neandertal haplotype at the OAS locus functionally impacts innate immune responses in humans. *Genome Biol* **17**: 246. doi:10.1186/s13059-016-1098-6
- Schiffels S, Haak W, Paajanen P, Llamas B, Popescu E, Loe L, Clarke R, Lyons A, Mortimer R, Sayer D, et al. 2016. Iron Age and Anglo-Saxon genomes from east England reveal British migration history. *Nat Commun* **7**: 10408. doi:10.1038/ncomms10408
- Ségurel L, Bon C. 2017. On the evolution of lactase persistence in humans. *Annu Rev Genomics Hum Genet* **18**: 297–319. doi:10.1146/annurev-genom-091416-035340
- Simcoe M, Valdes A, Liu F, Furlotte NA, Evans DM, Hemani G, Ring SM, Smith GD, Duffy DL, Zhu G, et al. 2021. Genome-wide association study in almost 195,000 individuals identifies 50 previously unidentified genetic loci for eye color. *Sci Adv* **7**: eabd1239. doi:10.1126/sciadv.abd1239
- Skoglund P, Mathieson I. 2018. Ancient genomics of modern humans: the first decade. *Annu Rev Genomics Hum Genet* **19**: 381–404. doi:10.1146/annurev-genom-083117-021749
- Skoglund P, Thompson JC, Prendergast ME, Mittnik A, Sirak K, Hajdinjak M, Salje T, Rohland N, Mallick S, Peltzer A, et al. 2017. Reconstructing prehistoric African population structure. *Cell* **171**: 59–71.e21. doi:10.1016/j.cell.2017.08.049
- Sohail M, Maier M, Ganna A, Bloemendal A, Martin AR, Turchin MC, Chiang CW, Hirschhorn J, Daly MJ, Patterson N, et al. 2019. Polygenic adaptation on height is overestimated due to uncorrected stratification in genome-wide association studies. *eLife* **8**: e39702. doi:10.7554/eLife.39702
- Steinrücken M, Bhaskar A, Song YS. 2014. A novel spectral method for inferring general diploid selection from time series genetic data. *Ann Appl Stat* **8**: 2203–2222. doi:10.1214/14-AOAS764
- Taal HR, Pourain BS, Thiering E, Das S, Mook-Kanamori DO, Warrington NM, Kaakinen M, Kreiner-Moller E, Bradfield JP, Freathy RM, et al. 2012. Common variants at 12q15 and 12q24 are associated with infant head circumference. *Nat Genet* **44**: 532–538. doi:10.1038/ng.2238
- Tataru P, Bataillon T, Hobolth A. 2015. Inference under a Wright-Fisher model using an accurate beta approximation. *Genetics* **201**: 1133–1141. doi:10.1534/genetics.115.179606
- Tataru P, Simonsen M, Bataillon T, Hobolth A. 2017. Statistical inference in the Wright-Fisher model using allele frequency data. *Syst Biol* **66**: e30–e46. doi:10.1093/sysbio/syw056
- Terhorst J, Schlötterer C, Song YS. 2015. Multi-locus analysis of genomic time series data from experimental evolution. *PLoS Genet* **11**: e1005069. doi:10.1371/journal.pgen.1005069
- Turchin MC, Chiang CW, Palmer CD, Sankararaman S, Reich D. Genetic Investigation of ANthropometric Traits (GIANT) Consortium, Hirschhorn JN. 2012. Evidence of widespread selection on standing variation in Europe at height-associated SNPs. *Nat Genet* **44**: 1015–1019. doi:10.1038/ng.2368
- Wang TJ, Zhang F, Richards JB, Kestenbaum B, van Meurs JB, Berry D, Kiel DP, Streeten EA, Ohlsson C, Koller DL, et al. 2010. Common genetic determinants of vitamin D insufficiency: a genome-wide association study. *Lancet* **376**: 180–188. doi:10.1016/S0140-6736(10)60588-0
- Wilde S, Timpons A, Kirsanow K, Kaiser E, Kayser M, Unterländer M, Hollfelder N, Potekhina ID, Schier W, Thomas MG, et al. 2014. Direct evidence for positive selection of skin, hair, and eye pigmentation in Europeans during the last 5,000 y. *Proc Natl Acad Sci* **111**: 4832–4837. doi:10.1073/pnas.1316513111
- Wood AR, Esko T, Yang J, Vedantam S, Pers TH, Gustafsson S, Chu AY, Estrada K, Luan J, Kutalik Z, et al. 2014. Defining the role of common variation in the genomic and biological architecture of adult human height. *Nat Genet* **46**: 1173–1186. doi:10.1038/ng.3097
- Yin X, Low HQ, Wang L, Li Y, Ellinghaus E, Han J, Estivill X, Sun L, Zuo X, Shen C, et al. 2015. Genome-wide meta-analysis identifies multiple novel associations and ethnic heterogeneity of psoriasis susceptibility. *Nat Commun* **6**: 6916. doi:10.1038/ncomms7916

Received April 24, 2022; accepted in revised form August 29, 2022.